# Dalton Transactions

Accepted Manuscript






ROYAL SOCIETY OF CHEMISTRY

www.rsc.org/dalton

Cite this: DOI: 10.1039/c0xx00000x

www.rsc.org/xxxxxx

ARTICLE TYPE

# Amorphous $Co_3O_4$ Modified CdS Nanorods with Enhanced Visible-light Photocatalytic $H_2$-production Activity

Jielin Yuan,[‡] Jiuqing Wen,[‡] Qiongzhi Gao, Shangchao Chen, Jiaming Li, Xin Li,[*] Yueping Fang[*]

***Received (in XXX, XXX) Xth XXXXXXXXX 20XX, Accepted Xth XXXXXXXXX 20XX***
**DOI: 10.1039/b000000x**

In this work, amorphous $Co_3O_4$ modified CdS nanorods were synthesized by a two-step solvothermal/hydrothermal method, and characterized by transmission electron microscopy (TEM), X-ray diffraction (XRD), high-resolution transmission electron microscopy, UV-visible spectroscopy, nitrogen absorption and X-ray photoelectron spectroscopy. The photocatalytic performance of the as-synthesized $Co_3O_4$-CdS nanorods was evaluated through $H_2$ generation from an aqueous solution containing sulfide and sulfite under visible light ($\lambda \geq 420$ nm). The results showed that the photocatalytic activity of CdS nanorods for $H_2$ evolution could be significantly enhanced by loading the amorphous $Co_3O_4$. The optimal $Co_3O_4$ loading was found to be approximately 3.0 mol %. The as-prepared CdS nanorods with 3 mol % $Co_3O_4$ exhibited the highest photocatalytic activity for $H_2$ evolution, 236 $\mu mol \cdot g^{-1} \cdot h^{-1}$ under visible light, which is 33-fold higher than that of the pristine CdS nanorods. Furthermore, the co-loading of 1% Pt can lead to another three times enhancement in the photocatalytic $H_2$-production activity. The mechanism for the enhanced $H_2$-production performance of $Co_3O_4$-CdS nanorods was discussed. The excellent performance of $Co_3O_4$-CdS nanorods is mainly ascribed to the loading of amorphous $Co_3O_4$ onto the surface of CdS nanorods, which could promote the separation of electron–hole pairs and enhance the stability of CdS nanorods due to the formation of p-n heterojunctions between $Co_3O_4$ and CdS nanorods, thus leading to an enhanced activity for $H_2$ generation. This work demonstrated that the loading of amorphous $Co_3O_4$ is a facile strategy to enhance the photocatalytic activity of CdS nanorods, which may provide some potential opportunities for designing other composite photocatalysts for water splitting.

## 1. Introduction

Due to the depletion of fossil fuel and serious environmental problems, much effort has been devoted to exploiting renewable, carbon-free energy sources, such as solar energy. As a direct, environmentally friendly and economic pathway for converting the sunlight energy into hydrogen energy, the photocatalytic production of hydrogen from water by means of solar energy and semiconductors has drawn a lot of attention and has proven to be a promising strategy for solving the global energy crisis and environmental pollution.[1] Since Fujishima and Honda for the first time reported photoelectrochemical water splitting on a $TiO_2$ electrode[2], numerous attempts have focused on the photocatalytic water splitting in the past decade years.[1, 3, 4] The current challenge is to split water efficiently using visible-light photocatalysts with long term stability, which had been described as one of the "Holy Grails" of chemistry.[5] To achieve visible light water splitting, the photocatalysts should have a proper band gap (1.8-2.2 eV)[6] for visible light absorption and an enough redox potentials for both hydrogen evolution and water oxidation. [3]

Among all the visible-light-driven photocatalysts, n-type semiconductor CdS appears to be one of the most promising materials for hydrogen evolution from aqueous solutions due to its relatively narrow band gap (Eg≈2.40 eV)[7] for absorption of visible light, and sufficient flat-band potential (-0.9 V vs. NHE)[8-11] for reduction of $H^+$ to $H_2$. However, CdS is not stable in aqueous media and exhibits very low photocatalytic activities in hydrogen production in the absence of noble metal as co-catalysts.[12] Therefore, to solve these problems, different strategies such as the control of crystalline phase and morphology,[13] formation of nano-structured CdS[14, 15] or the heterojunction,[16-24] the loading of co-catalysts[25-27] and nano-carbon materials[28], have been applied to modify the pristine CdS, which can greatly improve the bulk/surface $e^-/h^+$ separation and increase the surface active sites for hydrogen evolution, thus leading to an enhanced activity for water splitting. Despite the progress, a facile, scalable and cheap strategy is still highly desired for synthesizing CdS-based composite with enhanced activity for efficient solar hydrogen generation.

Recently, the earth-abundant cobalt-based electrocatalysts such as $CoO_x$,[29] CoS[25] and $Co(OH)_2$[30] have been found to founction as a co-catalysts for improving the photocatalytic $H_2$-evolution activity of CdS. For example, it was demonstrated that a 5-time enhancement in $H_2$-evolution activity could be achieved by loading a proper amount of CoS onto CdS although its increase in the activity is significantly smaller than that of NiS-

loaded CdS.[25] In another report, Zhang et al. found that a 41-time enhancement in $H_2$-evolution activity could be realized by loading 6.8 mol % $Co(OH)_2$ onto the CdS nanorods.[30] The results further revealed that the $Co(OH)_2$ nanoparticles could capture the photo-generated electrons and promote the $H_2$-generation activity as a potential electrocatalyst. In addition, the loading of 2.1 wt% $CoO_x$ onto $TiO_2$/CdS composite could enhance the photocatalytic activity for $H_2$ evolution by a factor of 7 times as compared to those of the $TiO_2$/CdS and CdS photocatalysts in the mixed solution of $Na_2S$ and $Na_2SO_3$ under visible light irradiation ($\lambda$>400 nm).[29] More recently, it was also reported that the layered films of CdS nanorods modified with $Co_3O_4$ nanoparticles exhibited good photoactivity for water oxidation and methylene blue reduction in solution.[31] To the best of our knowledge, there has been no report regarding the application of $Co_3O_4$/CdS composite materials in the field of photocatalytic hydrogen generation. Therefore, it would be of great interest to enhance the photocatalytic hydrogen evolution of CdS nanorods (NRs) through loading the $Co_3O_4$ co-catalysts.

In the present study, amorphous $Co_3O_4$ modified CdS nanorod photocatalysts were synthesized by a two-step solvothermal/hydrothermal method. The results demonstrate that the activity of the CdS NRs for $H_2$ evolution is significantly enhanced in the presence of the $Co_3O_4$ co-catalyst under visible light irradiation from an aqueous solution containing sulfide and sulfite. A possible enhancement mechanism for the improved photocatalytic activity of CdS-$Co_3O_4$ photocatalysts was also proposed and discussed.

## 2. Experimental Section

### 2.1. Preparation of photocatalysts

All chemicals were reagent grade and used without further purification. The pure CdS nanorod photocatalyst was synthesized by a one-step solvothermal reaction.[32] In a typical synthesis run, 3.86 g of $Cd(NO_3)_2.4H_2O$ and 2.85 g of thiourea ($NH_2CSNH_2$) were added into an autoclave with an inner Teflon lining (50 mL) which had been filled with ethylenediamine to 70% of its capacity (35 mL) and maintained at 160 ºC for 24 hours. After that, the yellow precipitates were collected by centrifuge, washed with distilled water and ethanol for three times, and then dried in an oven at 60 ºC for 10 h.

The loading of amorphous $Co_3O_4$ nanoparticles onto CdS NRs was also carried out by a hydrothermal route. 1 g of as-prepared CdS nanorods was introduced into a beaker containing 12.5 mL of deionized water and 20.0 mL of ethanol. Then 0.0202 g (0.0606 g or 0.1011 g) of $Co(NO_3)_2.6H_2O$ was added into this solution. The pH of the solution was adjusted to 9 by the addition of $NH_4OH$, and the resultant mixture was stirred continuously for 10 min at room temperature. After stirring, the solution was maintained at 160 ºC for 6 h in a Teflon autoclave in the oven. The final obtained products were washed with deionized water for three times, and then dried in an oven at 80 ºC. The molar ratio for Co/Cd in the initial photocatalyst precursors were 1, 3, and 5%, respectively. The final products were designated as CdS-1%$Co_3O_4$, CdS-3%$Co_3O_4$ and CdS-5%$Co_3O_4$, respectively. The *in-suit* loading of 1 wt % Pt cocatalyst was performed by directly dissolving $H_2PtCl_6$ into the photocatalytic systems before irradiation.

### 2.2. Characterization

The crystal structure of samples was investigated using X-ray diffraction (XRD; Rigaka D/max 2500v/pc X-ray diffractometer) with Cu Ka radiation at a scan rate of 4 °$min^{-1}$. The X-ray photoelectron spectroscopy (XPS) was performed with a VG ESCALAB250 surface analysis system using a monochromatized Al K$\alpha$X-ray source (300 W, 5 mA, and 15 kV). The base pressure was about 3 x $10^{-9}$ mbar. The shift of the binding energy owing to relative surface charging was corrected using the C 1s level at 284.6 eV as an internal standard. The elemental distribution at the micro scale was also investigated by Scanning Electron Microscope (SEM) and Energy dispersive X-ray spectrometry (Bruker AXS Microanalysis GmbH). The UV–visible absorption was measured by using a UV–vis spectrophotometer (TU1901, China). The specific surface area was determined by the Brunauer–Emmett–Teller (BET) method at 77 K. Nitrogen adsorption–desorption isotherms were measured on a Quantachrome NOVA1000 Sorptomatic apparatus. Transmission electron microscopy (TEM)images, high-resolution transmission electron microscopy (HRTEM)images, and selected area electron diffraction (SAED) patterns were collected on an F20 S-TWIN electron microscope (Tecnai G2,FEI Co.), using a 200 kV accelerating voltage.. The photoluminescence (PL) spectra were checked by using LS 50B (Perkin Elmer, Inc., USA).

### 2.3. Photocatalytic reaction procedures

Photocatalytic water splitting was carried out in a LabSolar $H_2$ photocatalytic hydrogen evolution system (Perfectlight, Beijing) including a 300 W Xe lamp (PLS-SXE300, Beijing Trusttech). In a typical photocatalytic reaction, 50 mg of powder sample was dispersed in an aqueous solution (100 mL) containing 0.5 M $Na_2S$ and 0.5 M $Na_2SO_3$. Then the system was sealed and vacuumized to keep the pressure as-0.1 MPa. Afterwards, a circular cooling water system was turned on and the reactor was irradiated with Xe lamp (300 W) with a UV cut-off filter ($\lambda\geq$420 nm) under magnetic stirring. The gases evolved were analyzed on line with a gas chromatograph (GC-7900, TCD, with $N_2$ as carrier gas) after 0.5 h of illumination. The reaction was continued for 3 h.

## 3. Results and Discussion

### 3.1 X-ray Diffraction (XRD).

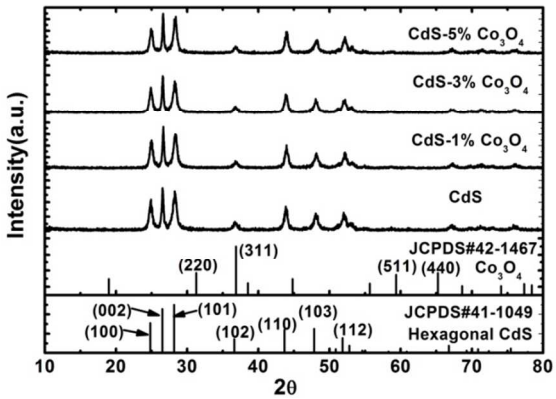


Figure 1 XRD patterns of pure CdS and the CdS-$Co_3O_4$ composite photocatalysts.

The crystal phase structure of samples was investigated by XRD measurements. Fig. 1 shows that XRD patterns of pure CdS and CdS-$Co_3O_4$ photocatalysts with different percentage of $Co_3O_4$. As shown in Fig. 1, it is clear that all samples possess similar XRD patterns, exhibiting diffraction peaks of hexagonal

CdS phase with lattice parameters a = 4.14 Å and c = 6.72 Å. The peaks at 2θ values of 24.81°, 26.51°, 28.18°,36.62°,43.68°, 47.84°and 51.82° were assigned to the (100), (002), (101), (102), (110), (103) and (112) crystal planes of CdS (JCPDS#41-1049), respectively, indicating that well-crystallized CdS was successfully synthesized. It is known that the hexagonal CdS with good crystallinity exhibits better photoactivity for $H_2$ evolution than the cubic one.[12] Thus, the hexagonal crystal phase may favor the enhancement of photocatalytic $H_2$-evoluion activity. In addition, no apparent peaks corresponding to $Co_3O_4$ species were observed in $Co_3O_4$/CdS composites as compared with pure CdS, due to the low content and high dispersion of $Co_3O_4$ in the composites. Therefore, the results suggest that the deposition of $Co_3O_4$ did not affect the crystalline structure of CdS.

### 3.2 X-ray Photoelectron Spectroscopy (XPS)

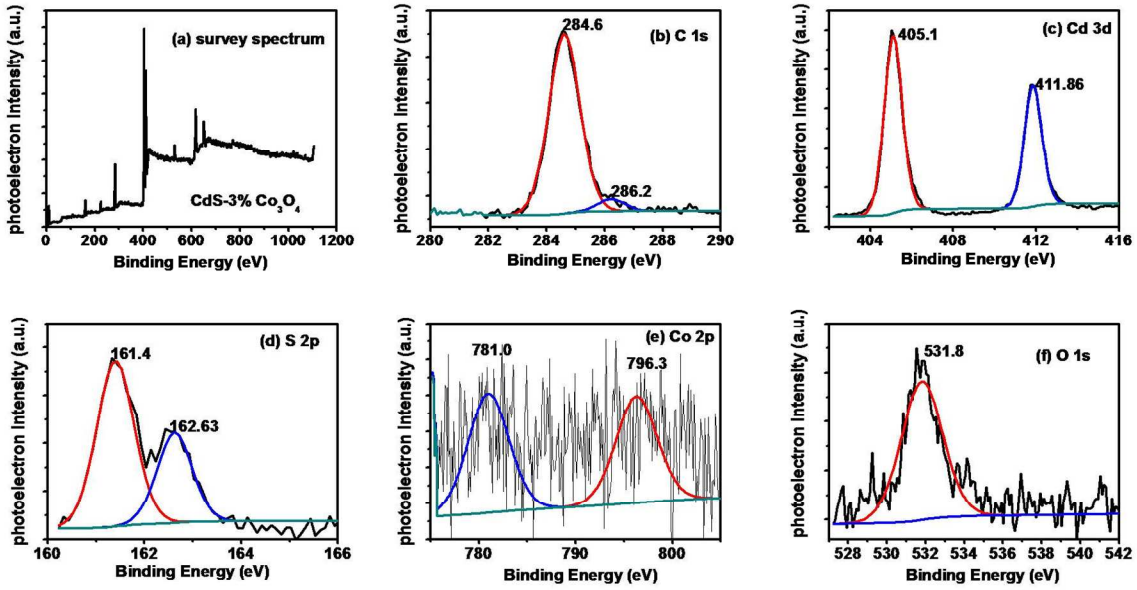


Fig. 2. XPS spectrum of the as-prepared CdS-3% $Co_3O_4$ composite photocatalyst: (a) survey spectrum; (b) C 1s; (c) Cd 3d; (d)S 2p; (e) Co 2p; (f) O 1s.

To identify the chemical composition and oxidation state of different atoms in the composite particles, the X-ray photoelectron spectroscopy (XPS) of the composite particles with 3 mol% cobalt content was measured. Fig. 2a presents the survey scan XPS spectrum of the sample. The binding energies obtained in the XPS analysis were corrected for specimen charging by referencing C 1s to 284.60eV. XPS peaks in Fig. 2a indicated the presence of Cd, O, C, S and Co elements. Fig. 2b shows the high-resolution XPS spectra of C 1s. The photoelectron peak at 286.2 eV for C 1s may originate from absorbed gaseous molecules. The High resolution XPS spectra of Cd 3d, S 2p, Co 2p and O 1s core level for the CdS-3%$Co_3O_4$ sample were shown in Fig. 2c, d, e and f, respectively. The Cd $3d_{5/2}$ and Cd $3d_{3/2}$ peaks located at 405.1 eV and 411.85 eV with a spin–orbit separation of 6.7 eV, are consistent with the reported values for CdS.[33] The binding energies of S $2p_{3/2}$ and S $2p_{1/2}$ are 161.4 eV and 162.63 eV, respectively, which are very close to the published values in literature.[34, 35] There is no $SO_4^{2-}$ as an impurity on the surface of CdS NRs because there were no obvious peaks nearby the 168 eV.[36] It is observed from Fig. 2e that the Co 2p XPS spectrum of the composite exhibits two weak peaks at 796.3 eV and 781.0eV, corresponding to the Co $2p_{1/2}$ and Co $2p_{3/2}$ spin orbit, due to the low loading of $Co_3O_4$. In addition, the O 1s XPS peak at 531.85eV corresponds to the lattice oxygen in the $Co_3O_4$ phase, further confirming the existence of $Co_3O_4$.[37, 38] The measured atomic concentrations through XPS are 4.69%, 10.23%, 12.40%, 0.40% and 72.08% for O, S, Cd, Co and C, respectively. The molar ratio of Co/Cd is 3.23%, which is very close to the exprimental design value (3%). Although XPS results provide some important information about $Co_3O_4$, further investigation is to fully confirm the existence of $Co_3O_4$ in the as-prepared composite photocatalysts.

### 3.3 TEM and EDX characterization

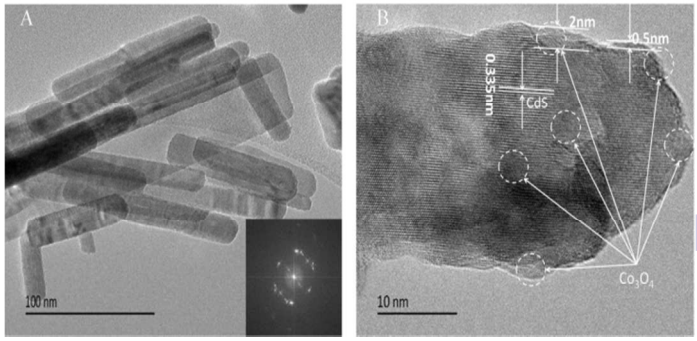


**Fig. 3** (A) TEM (inside picture, SAED pattern) and (B) HRTEM images of as-prepared CdS-3% $Co_3O_4$ sample.

The structural information of the photocatalysts was further identified by TEM and HR-TEM. Fig. 3 shows the TEM and HRTEM image of the CdS-3% $Co_3O_4$ sample. From the TEM pictures in Fig. 3A, it could be clearly seen that the CdS sample is composed of a large quantity of uniformly distributed CdS NRs with an average diameter of approximately 40–60 nm and length of 100-500 nm. An obvious aggregation of these CdS NRs is also observed. Since the effective diffusion length of electron in CdS

is about 0.65μm,[39] thus, the hot electrons in these CdS NRs have enough time to reach the surface of CdS NRs and participate in the photocatalysis reaction. The SAED pattern shown in the inset of Fig. 3A indicates that the CdS NR is a single phase (hexagonal) CdS with a high crystallinity and a growth direction along the *c* axis. As shown in Fig. 3B, the HRTEM image of the CdS-3% $Co_3O_4$ sample clearly exhibits fringes with lattice spacing of 0.335 nm, which correspond to the (002) lattice plane of the typical hexagonal CdS.[40] Furthermore, it was clearly observed that the diameter of $Co_3O_4$ nanoparticles on the surface of CdS NRs was about 0.5–2 nm. However, it is difficult to found obvious lattice fringes of $Co_3O_4$ nanoparticles, suggesting the formation of amorphous $Co_3O_4$ nanoparticles on the surface of CdS NRs.

The elemental distributions of Cd, Co, S and O at the micro scale were also determined by the SEM-EDX mapping. The corresponding results are shown in Fig. 4. Fig. 4a presents the microscaled SEM image. The signals of S, Co, Cd and O elements are clearly shown in Fig. 4b-f for the selected area in Fig. 4a. Especially, highly dispersed Co element with quite low density can also be clearly observed from Fig. 4d. It can be seen from Fig. 4g that the EDX peaks of Co were detected on the CdS NRs, confirming the presence of the $Co_3O_4$ nanoparticles on the CdS NRs. The molar ratio of Co/Cd is 1.08%, which is much smaller than the design value (3%), suggesting that the $Co_3O_4$ nanoparticles are mainly loaded on the surface of CdS NRs. These results further confirm the presence of $Co_3O_4$ in the composite photocatalysts.

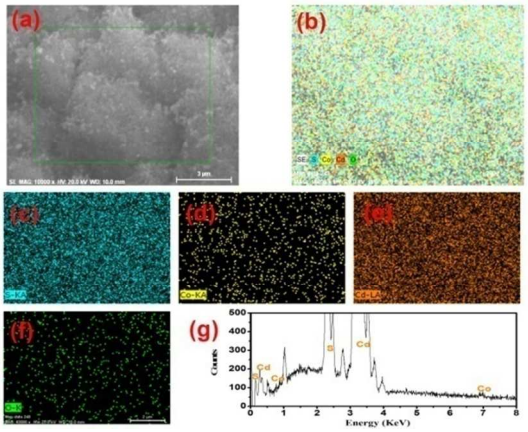


Fig. 4 (a) SEM image, (b-f) the corresponding EDX mapping and (g) EDX spectrum of the CdS-3% $Co_3O_4$ photocatalyst at the region shown in (a).

### 3.4 UV-visible absorption spectra and textural properties

The optical properties of the as-prepared pure CdS and CdS-$Co_3O_4$ composite samples were measured using UV−vis absorption spectra. Fig. 5 depicts the UV−vis absorption spectra for all samples. As shown in Fig. 5, the CdS sample has photo-absorption from UV light to visible light. The pure CdS shows an absorption edge at about 525 nm. The optical band gap energy ($E_g$) was estimated to be about 2.37 eV by the Tauc plot,[41] which agrees well with the reported values.[42] Furthermore, $Co_3O_4$ deposition has significant influences on the optical absorption of CdS NRs. Notably, the ability of visible light absorption in the region from 600 to 800 nm for CdS-$Co_3O_4$ composite photocatalysts was significantly enhanced, due to the strong absorption of $Co_3O_4$ species in the composite photocatalysts. It is known that $Co_3O_4$ is a multifunctional spinel-type p-type semiconductor with two small band gaps (~1.45 and 2.07 eV),[43] which correspond to the $O^{2-} \rightarrow Co^{2+}$ and $O^{2-} \rightarrow Co^{3+}$ transitions, respectively.[44] The similar enhancements of visible-light absorption in this region were also observed in the systems of $Co_3O_4/Bi_2WO_6$[38], $Co_3O_4/C_3N_4$[44] and $Co_3O_4/BiVO_4$[43] due to the loading of $Co_3O_4$ species. Further observation shows that almost all composite photocatalysts exhibit the same band gap energy as that of pure CdS, demonstrating that $Co_3O_4$ species were not incorporated into the CdS lattice. In addition, it was also seen that only a little enhancement for visible light absorption was observed with increasing the content of $Co_3O_4$ in the composites, which was due to the low loading amounts of $Co_3O_4$ species. These results clearly confirmed that the presence of $Co_3O_4$ species can enhance the visible-light absorption of CdS NRs, which may lead to a higher photocatalytic activity.

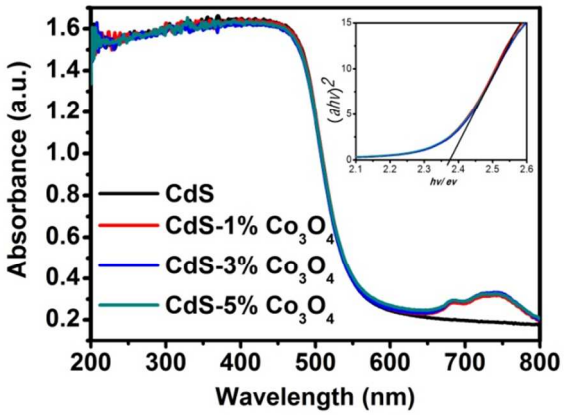


**Fig. 5** UV-vis absorption spectra of the as-prepared pure CdS and CdS-$Co_3O_4$ composite samples.

The surface areas and porous structures of CdS and CdS-3% $Co_3O_4$ samples were also investigated by nitrogen adsorption. Fig. 6 gives the adsorption–desorption isotherms of $N_2$ and the corresponding pore size distribution curves (inset) of the CdS and CdS-3% $Co_3O_4$ samples. As observed in Fig. 6, the two tested samples show type-IV adsorption-desorption isotherms according to the IUPAC classification.[45] Each isotherm shows a distinct H3 hysteresis loop in a relative pressure range of 0.9-1. Generally, it is believed that the H3 hysteresis loop is related to the mesopores through the aggregates of plate-like particles.[45] However, there have been no plate-like particles in this system. Thus, the mesopores may come from the random aggregation of CdS NRs, which were further observed from the corresponding pore size distribution curves (shown in the inset of Fig 6). The structure parameters of the photocatalysts are summarized in Table 1. It is also observed from Table 1 that the average pore diameter of the CdS-3% $Co_3O_4$ photocatalyst almost equals to that of pure CdS NRs, suggesting that the mesoporous structure is not the main factor in enhancing the photocatalytic activity. The obtained BET specific surface area of the CdS-3% $Co_3O_4$ sample is 38.81 $m^2.g^{-1}$, whereas that of CdS sample is 32.68 $m^2.g^{-1}$, respectively. Accordingly, it is clear that the BET surface area of the CdS-3% $Co_3O_4$ photocatalyst is a little larger than that of pure CdS NRs.

This can be attributed to the formation of amorphous $Co_3O_4$ nanoparticles on the surface of CdS NRs rather than in the pores. The increased surface area may be also beneficial for the increase of active sites and photoactivities.

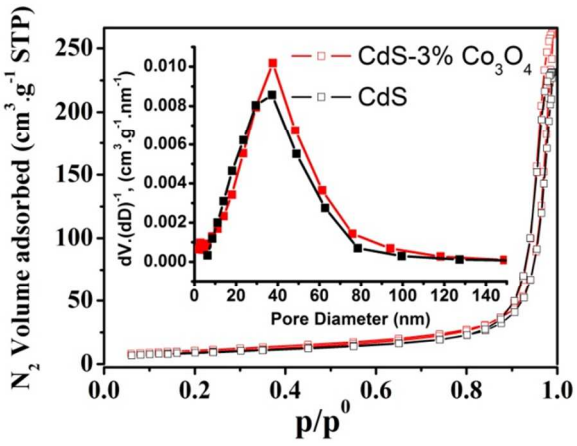


**Fig. 6** Nitrogen adsorption-desorption isotherms and corresponding pore-size distribution curves (inset) of CdS and CdS-3% $Co_3O_4$ samples.

Table 1. Porous structure parameters of CdS and CdS-3% $Co_3O_4$ samples

| Photocatalysts | BET surface area ($m^2.g^{-1}$) | Mean pore diameter (nm) | Pore volume ($cm^3.g^{-1}$) |
|---|---|---|---|
| CdS | 32.68 | 32.35 | 0.36 |
| CdS-3% $Co_3O_4$ | 38.81 | 32.89 | 0.41 |

### 3.5 Photocatalytic hydrogen production

No substantial $H_2$ evolution could be detected in control experiments such as no photocatalysts or non-irradiation, indicating that $H_2$ was produced through the photocatalytic reactions rather than the mechanocatalytic water splitting.[46] The photocatalytic activities over various photocatalysts for hydrogen production are shown in Fig. 7A. As shown in Fig. 7A, during the 3-h photocatalytic reaction process, the average rates of hydrogen evolution were determined to be 7.3, 115.9, 236.3 and 39.3 $\mu mol \cdot g^{-1} \cdot h^{-1}$ for CdS, CdS-1% $Co_3O_4$, CdS-3% $Co_3O_4$ and CdS-5% $Co_3O_4$, respectively. It is obvious that all of three composite photocatalysts exhibit better photoactivities than the pure CdS photocatalyst. Especially, the CdS-3% $Co_3O_4$ shows a 33-fold increase in the average rate of hydrogen evolution as compared to the pure CdS photocatalyst, which is also about 6 times and 2 times larger than those of CdS-5% $Co_3O_4$ and CdS-1% $Co_3O_4$, respectively. It is clear that the photocatalytic activities first increased and then decreased as the increase of $Co_3O_4$ species content. The possible reasons are that proper amounts of $Co_3O_4$ can act as co-catalysts to enhance the separation of holes and electrons, thus leading to an enhanced photocatlytic activity for $H_2$ evolution over CdS photocatalyst, while the modification with excessive $Co_3O_4$ (>3 mol%) nanoparticle can lead to a decrease in the activity due to the masking effect of active sites. From these results, it can be concluded that the amorphous $Co_3O_4$ nanoparticles on the surface of CdS may play a key role in dramatically enhancing the hydrogen evolution efficiency. In addition, it should be noted that the amount of $H_2$ evolved in the first half hour is lower than that in the later reaction, indicating the existence of an induced period. This is because the internal electric fields in the p-n heterojunction between $Co_3O_4$ and CdS will be gradually formed during this period,[47] which will be discussed in the following section.

To better understand the promoting roles of amorphous $Co_3O_4$ in enhancing the $H_2$ evolution rate of CdS NRs. Some famous CdS-based photocatalyst systems for $H_2$ production were summarized in Table 2. As observed in Table 2, there is a significant difference in their activities for $H_2$ production. It is known that their activities for $H_2$ production are strongly dependant on the controlled experimental conditions such as a light source with different intensity and frequency, and a type of a reaction cell or sacrificial reagent.[48] Generally, a strong light source with high intensity and a highly effective sacrificial reagent could lead to an enhanced activity. Thus, for a fairer comparison of the promoting roles of co-catalysts, an enhanced factor for different systems is also provided in Table 3. Clearly, although a 33-fold activity increase of CdS-3% $Co_3O_4$ for $H_2$ production is significantly lower than those of some famous systems such as CdS/$Ni(OH)_2$,[49] CdS/$NiO_x$,[50] CdS-RGO-$MoS_2$,[51, 52] and Pt-PdS-CdS, [53] it is very close to those reported for CdS/$MoS_2$,[51] CdS-RGO-Pt,[28] CdS/NiS,[25, 40] CdS/$Co(OH)_2$[30] and CdS/$WS_2$. [54] Note that, Co is an earth-abundant element. These comparisons further indicate that the amorphous $Co_3O_4$ is a promising candidate as a highly efficient co-catalyst due to its positive effects for photocatalytic $H_2$ production.

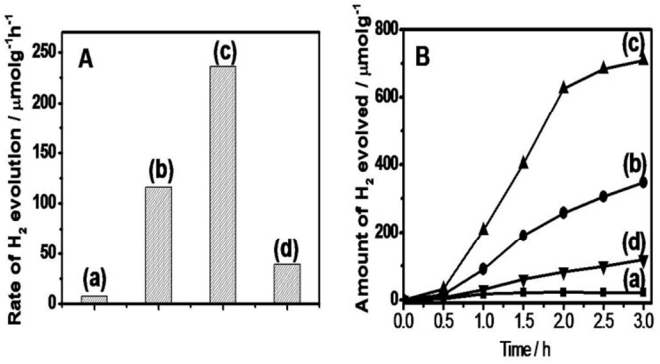


Fig. 7 (A) The average rate of $H_2$ evolution and (B) Time courses of photocatalytic $H_2$ evolution over the photocatalysts: (a) CdS; (b) CdS-1% $Co_3O_4$; (c) CdS-3% $Co_3O_4$; (d) CdS-5% $Co_3O_4$. Reaction conditions: catalyst, 0.05 g; 0.5 M $Na_2S$ and 0.5 M $Na_2SO_3$ solution, 100 mL; light source, xenon lamp (300 W) with a UV cut-off filter ($\lambda \geq 420$ nm).

Table 2 Comparison of the CdS-3% $Co_3O_4$ sample with other famous CdS-based photocatalysts for their $H_2$-production activities

| Photocatalyst | Synthesis method | Co-catalyst | Light source | Sacrificial reagent | Activity ($\mu mol\ g^{-1}\ h^{-1}$) | Enhanced factor | Ref.(Year) |
|---|---|---|---|---|---|---|---|
| CdS NRs | solvothermal/ hydrothermal | 3 mol % $Co_3O_4$ | 300 W Xe-lamp, $\lambda \geq 400$ nm | 0.5 M $Na_2S$ and 0.5 M $Na_2SO_3$ | 236 | 33 | this work |
| CdS NRs | coprecipitation | 6.8 mol % $Co(OH)_2$ | 500 W Xe | 25vol%ethanol | 61 | 41 | [30](2014) |
| CdS/$TiO_2$ | solvothermal | 2.1 wt%$CoO_x$ | 300 W Xe-lamp, $\lambda \geq 400$ nm | 0.125 M $Na_2S$ + 0.175 M $Na_2SO_3$ | 660 | 7 | [29](2014) |
| CdS | hydrothermal | CoS | 300 W Xe-lamp, $\lambda \geq 420$ nm | 30 vol% lactic acid | 1050 | 5 | [25](2010) |
| CdS | Impregnation-sulfidation | 0.2 wt% $MoS_2$ | 300 W Xe-lamp, $\lambda \geq 420$ nm | 10 vol % lactic acid | ~5400 | 36 | [51](2008) |
| CdS | hydrothermal | 1.33 wt% grapheme,0.67 wt% $MoS_2$ | 300 W Xe-lamp, $\lambda \geq 420$ nm | 20 v% lactic acid | 9000 | 72 | [52](2014) |
| CdS | hydrothermal-mixing | 0.4 wt % RGO, 2 wt% $MoS_2$ | 500 W UV-vis lamp | 10 v% lactic acid | 6857 | 71 | [55](2014) |
| CdS | Impregnation-sulfidation | 1.0 wt % $WS_2$ | 300 W Xe-lamp, $\lambda \geq 420$ nm | 10 vol% lactic acid | ~4200 | 28 | [54](2011) |
| CdS | precipitation | 10 wt% WC | 500 W Hg-arc lamp, $\lambda > 420$ nm | 0.1 M $Na_2S$ and 0.02 M $Na_2SO_3$ | 1400 | 23 | [56](2008) |
| CdS | hydrothermal | 1.2 mol% NiS | 300 W Xe-lamp, $\lambda \geq 420$ nm | 30 vol% lactic acid | 7266 | 34 | [25](2010) |
| CdS NRs | solvothermal/ hydrothermal | 5 mol % NiS | 300 W Xe-lamp, $\lambda \geq 420$ nm | 0.35 M $Na_2S$ and 0.25 M $Na_2SO_3$ | 1131 | 20.6 | [40](2013) |
| CdS | precipitation | 23 mol% $Ni(OH)_2$ | 300 W Xe-lamp, $\lambda \geq 420$ nm | 25 v% triethanolamine | 5085 | 145 | [49](2011) |
| CdS | Hydrothermal | 1 mol% $NiO_X$ | 300 W Xe-lamp, $\lambda > 400$ nm | 30% Methanol | 5402 | 108 | [50](2014) |
| CdS NRs | solvothermal | 3 mol% CuS | 500 W Xe-lamp, | 0.35 M $Na_2S$ and 0.25 M $Na_2SO_3$ | 332 | 3.5 | [27](2013) |
| CdS | hydrothermal-photodeposition | 0.30 wt% Pt -0.13 wt% PdS | ≥420 nm | 0.5 M $Na_2S$ and 0.5 M $Na_2SO_3$ | 29 232 | *381* | [53](2009) |
| CdS | solvothermal | 1 wt% RGO ,0.5 wt% Pt | 350 W Xe-lamp, $\lambda \geq 420$ nm | 10 v% lactic acid | 56000 | 45.6 | [28](2011) |
| CdS | hydrothermal | 1 wt% Pt3Co | ≥ 420 nm | 10 v% lactic acid | 15890 | 13.8 | [26](2013) |

The time courses of $H_2$ evolution were showed in Fig. 7B. Obviously, the $H_2$ evolution rates of all composite photocatalysts show a significant increase during the whole photocatalytic reactions, except the pure CdS. For pure CdS, the yields of $H_2$ evolution can reach the maximum value, and then it lost its activity. It is explained that the morphology and crystal structure of the CdS NRs can be easily destroyed due to the photo-corrosion of CdS during photocatalytic processes.[42] To better evaluate the photostability of the $Co_3O_4$/CdS composites, the time courses of photocatalytic $H_2$ evolution of the CdS-3% $Co_3O_4$ sample as an example was measured every 3 h as one cycle. The corresponding results are shown in Fig. 8. It is clear that there is no significant decrease in activity for $H_2$ production after 3 cycles, indicating the introduction of amorphous $Co_3O_4$ nanoparticles can significantly enhance the stability of CdS sample under visible light irradiation. To further investigate the photostability, the characterization of CdS-3% $Co_3O_4$ photocatalyst after 3 runs of $H_2$ generation was carried out again. The TEM images of CdS-3% $Co_3O_4$ photocatalyst after the three-cycle test were given in **Fig. 9**. Clearly, the morphology and structure of nanorods are still similar to those before the reaction, suggesting the loading of $Co_3O_4$ is an effective strategy to improve the photostability of CdS NRs. The main cause of increased stability might be ascribed to the inhibited photocorrosion by accelerating the hole transfer from the valence band of CdS to the aqueous solution.

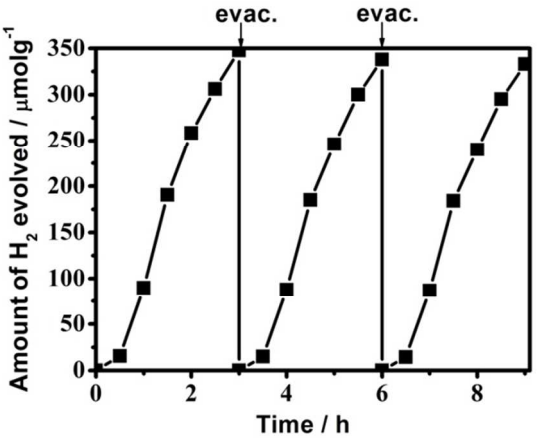


**Fig. 8** Repated time courses of photocatalytic $H_2$ evolution on CdS-3% $Co_3O_4$ sample. Reaction conditions: catalyst, 0.05 g; 0.5 M $Na_2S$ and 0.5 M $Na_2SO_3$ solution, 100 mL; light source, xenon lamp (300 W) with a UV cut-off filter ($\lambda \geq 420$ nm).

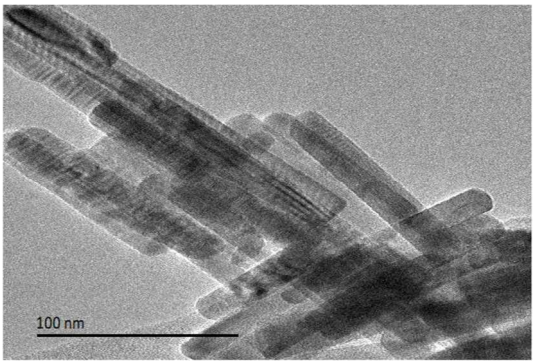


**Fig. 9** TEM images of the CdS-3% $Co_3O_4$ sample after the three-cycle test

### 3.6 Discussion of Mechanism

To further investigate the photocatalytic $H_2$-production mechanism over amorphous $Co_3O_4$ modified CdS NRs, the photoluminescence (PL) spectra of the photocatalysts was performed, which is useful to reveal the migration, transfer, and recombination processes of the photogenerated electron-hole pairs in the semiconductor.[37] Fig. 10 presents the PL spectra of pure CdS and the CdS-$Co_3O_4$ composite photocatalysts at an excitation wavelength of 260 nm. As expected, among the four samples, the CdS-3% $Co_3O_4$ sample showed the weakest intensity, whereas pure CdS NRs exhibited the strongest intensity. The intensity of CdS-5% $Co_3O_4$ sample is a little lower than that of CdS-1% $Co_3O_4$ sample. The results are in very good agreement with the photocatalytic activities and our above discussions. Thus, the separation of photo-generated charge carriers is crucial to the enhancements in the photoactivities and studies of mechanism.

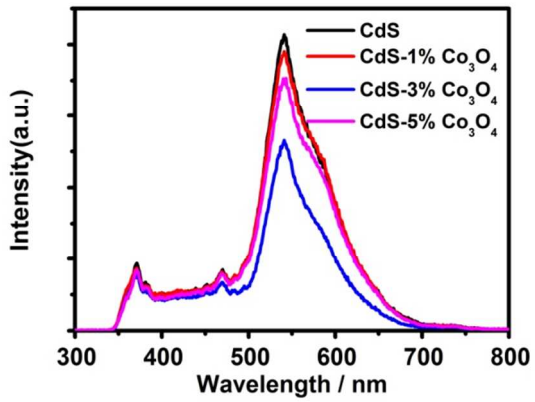


Fig. 10 PL spectra of pure CdS, as well as of the composite photocatalysts at an excitation wavelength of 260 nm

On the basis of the PL and photocatalytic activity results, a possible mechanism for the photocatalytic hydrogen evolution using the composite photocatalysts is proposed. The schematic diagram of photocatalytic hydrogen evolution over composite photocatalysts under visible light irradiation is illustrated in Fig. 11. On the one hand, $Co_3O_4$ is a p-type semiconductor, whereas CdS is an n-type material. Once the two types of semiconductor materials are combined together, a p-n heterojunction would be formed at the interfaces between $Co_3O_4$ and CdS. The migration of photogenerated holes to the valence band of $Co_3O_4$ can be promoted by the internal field, leaving the holes in the conduction band of CdS. It should be noted that the hole transport from the CdS NRs to the $Co_3O_4$ has been recently demonstrated by Yehezkeli and co-workers through electrochemical and photoelectrochemical studies.[31] Clearly, such a fast hole transport will greatly reduce the recombination of electron-hole pairs, thus leading to enhanced stability of the CdS and improved $H_2$ evolution rate. On the other hand, it is reported that a robust electrocatalyst $Co_3O_4$ has been extensively used in electrocatalytic water oxidation.[57] More interestingly, it was revealed recently that the $Co_3O_4$ nanoparticles can also be employed to accelerate the photocatalytic $H_2$-generation rate as cocatalysts and enhance the proton-reduction activity as active electrocatalysts.[29, 58] Therefore, there is no doubt that the formation of $Co_3O_4$/CdS junctions plays very important roles in enhancing the photocatalytic activity for $H_2$-production, which not only promotes the charge separation rate, but also allows for the improvements in the $H_2$-evolution kinetics as co-catalysts. In addition, no significantly increased $H_2$-evolvtion rate was observed for the physical mixture systems of CdS NRs and amorphous $Co_3O_4$ as compared to that of pure CdS NRs, further indicating the key roles of a p-n heterojunction between $Co_3O_4$ and CdS in enhancing the photoactivity. As shown in Fig. 11, the photo-generated holes not only migrate to the surface of CdS NRs to oxidize the sacrificial reagents, but also to the $Co_3O_4$ to promote the oxidation of sacrificial reagents under visible light. Therefore, we propose that the $Co_3O_4$ on the surface of CdS nanorods can enhance the consumption rate of the photo-generated holes, further leading to the increase in the concentration of photo-generated electrons in CdS. Thus, the $H_2$-evolution rate and stability can be greatly improved due to the enhanced separation of electron–hole pairs.

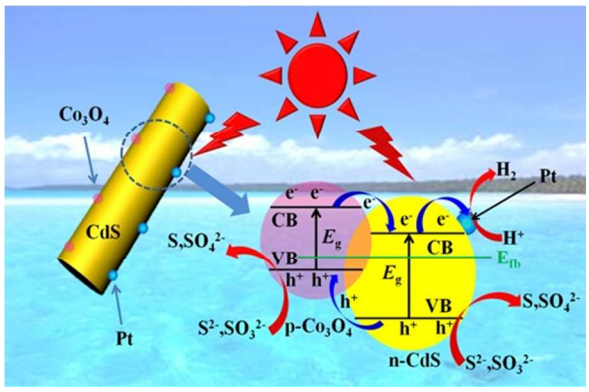


**Fig. 11** The schematic diagram of photocatalytic hydrogen evolution over CdS-$Co_3O_4$ composite photocatalysts under visible light irradiation.

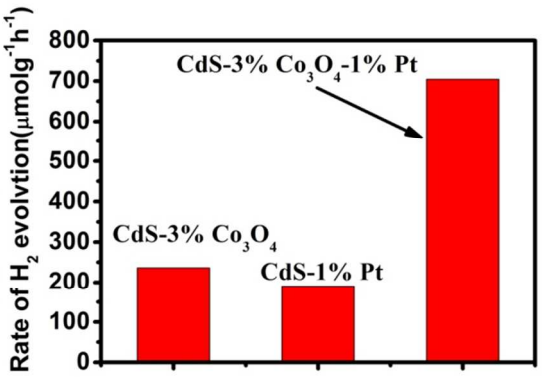


**Fig. 12** Comparison of the photocatalytic $H_2$-evolvtion rate of the CdS-3%$Co_3O_4$, CdS-1% Pt and CdS-3% $Co_3O_4$-1% Pt samples under visible light irradiation. Reaction conditions: catalyst, 0.05 g; 0.5 M $Na_2S$ and 0.5 M $Na_2SO_3$ solution, 100 mL; light source, xenon lamp (300 W) with a UV cut-off filter (λ≥420 nm).

Pt is generally loaded on the photocatalyst as a very efficient co-catalyst for photocatalytic $H_2$ production due to its high activity and low overpotential for $H_2$ evolution reaction.[59] To further enhance the photocatalytic activity for $H_2$ evolution, Pt was loaded on $Co_3O_4$/CdS photocatalysts by *in-suit* photodeposition.[60] Fig. 12 displays a comparison of the photocatalytic $H_2$-production activity of CdS-3% $Co_3O_4$, CdS-1% Pt and CdS-3% $Co_3O_4$-1% Pt samples under visible light irradiation. Surprisingly, as shown in Fig. 12, the $H_2$ evolution rate (236.3 μmol·g$^{-1}$·h$^{-1}$) over the CdS-3% $Co_3O_4$ sample is even much higher than that (190.3 μmol·g$^{-1}$·h$^{-1}$) for the best known Pt/CdS photocatalyst for hydrogen production under visible light. Considering its lower cost and ready availability, $Co_3O_4$ has great potential to be used as $H_2$-evolution co-catalysts for CdS photocatalyst. Importantly, the highest activity for photocatalytic $H_2$ evolution (704.7 μmol·g$^{-1}$·h$^{-1}$) was observed by co-loading of both 1% Pt and 3% $Co_3O_4$ co-catalysts onto CdS photocatalyst due to the accumulative catalytic effects and rectified charge separation. This was because that Pt and $Co_3O_4$ could function as the electron transfer and hole transfer co-catalysts, respectively.

An efficient charge separation can be achieved by co-loading of 1 % Pt and 3% $Co_3O_4$ in the CdS NRs (as shown in Fig. 7). Thus, the resulting CdS-3% $Co_3O_4$-1% Pt sample showed a significantly enhanced photocatalytic activity for hydrogen evolution than the CdS-3% $Co_3O_4$ or CdS-1% Pt sample due to the suppressed recombination of electron-hole pairs and enhanced kinetics of water splitting. The results further confirmed that the co-loading of the electron and hole transfer co-catalysts is a promising strategy to develop highly efficient photocatalysts for water splitting. In future studies, it is also highly expected that the spatially separated dual co-catalysts can further improve the activity of CdS NRs for photocatalytic water splitting. [61]

## 4. Conclusions

In summary, amorphous $Co_3O_4$ modified CdS NRs composite photocatalysts can be easily fabricated by a two-step solvothermal/hydrothermal method. The CdS photocatalysts with a loading content of $Co_3O_4$ approximately 3.0 % (molar ration for Co/Cd), exhibited the highest photocatalytic activity for hydrogen evolution, 236 $\mu mol.g^{-1}.h^{-1}$, under solar light irradiation from an aqueous solution containing sulfide and sulfite. It is believed that the deposition of $Co_3O_4$ nanoparticles on the surface of CdS nanorods can enhance the consumption rate of the photo-generated holes, and further improve the separation of electron–hole pairs. Thus, the photocatalytic activity was greatly enhanced. Future work will be focused on optimizing the system by tuning particle size of $Co_3O_4$ and by replacing the Pt by earth-abundant co-catalyst such as $MoS_2$. This work indicates the earth-abundant $Co_3O_4$ has great potential to integrate with metal sulfides to promote the $H_2$ generation reactions.

## 5. Acknowledgements

X. Li would like to thank NSFC (20906034), the project (2015-KF-7) supported by State Key Laboratory of Advanced Technology for Material Synthesis and Processing (Wuhan University of Technology) and the key Academic Program of the 3rd phase “211Project” of South China Agricultural University (Grant No. 2009B010100001) for their support. Y. Fang would like to thank the National Natural Science Foundation of China (20963002 and 21173088) for their support. Special thanks to Prof. Can Li in State Key Laboratory of Catalysis, Dalian Institute of Chemical Physics, Chinese Academy of Sciences. This work also partly supported by the State Key Laboratory of Catalysis cooperation project (N-08-08).

## Notes and references

*College of Science, South China Agricultural University, Guangzhou 510642, China. E-mail: Xinliscau@yahoo.com (X. Li), ypfang@scau.edu.cn (Y. Fang)*

† Electronic Supplementary Information (ESI) available: [details of any supplementary information available should be included here]. See DOI: 10.1039/b000000x/

‡ Jielin Yuan and Jiuqing Wen contributed equally.

1. A. Fujishima, X. Zhang and D. A. Tryk, *Int. J. Hydrogen. Energ.*, 2007, 32, 2664-2672.
2. A. Fujishima and K. Honda, *Nature*, 1972, 238, 37-38.
3. Y. Moriya, T. Takata and K. Domen, *Coordin. Chem. Rev.*, 2013, 257, 1957-1969.
4. X. Chen, S. Shen, L. Guo and S. S. Mao, *Chem. Rev.*, 2010, 110, 6503-6570.
5. A. Bard and M. Fox, *Accounts. Chem. Res.*, 1995, 28, 141-145.
6. J. Nowotny, C. C. Sorrell, L. R. Sheppard and T. Bak, *Int. J. Hydrogen. Energ.*, 2005, 30, 521-544.
7. H. J. Yan, J. H. Yang, G. J. Ma, G. P. Wu, X. Zong, Z. B. Lei, J. Y. Shi and C. Li, *J. Catal.*, 2009, 266, 165-168.
8. X. Li, H. Liu, D. Luo, J. Li, Y. Huang, H. Li, Y. Fang, Y. Xu and L. Zhu, *Chem. Eng. J.*, 2012, 180, 151-158.
9. J. S. Jang, U. A. Joshi and J. S. Lee, *J. Phys. Chem. C*, 2007, 111, 13280-13287.
10. D. Jing and L. Guo, *J. Phys. Chem. B*, 2006, 110, 11139-11145.
11. X. Li, T. Xia, C. Xu, J. Murowchick and X. Chen, *Catal. Today*, 2014, 225, 64-73.
12. N. Bao, L. Shen, T. Takata, K. Domen, A. Gupta, K. Yanagisawa and C. A. Grimes, *J. Phys. Chem. C*, 2007, 111, 17527-17534.
13. D. Lang, Q. Xiang, G. Qiu, X. Feng and F. Liu, *Dalton Trans.*, 2014, 43, 7245-7253.
14. N. Bao, L. Shen, T. Takata and K. Domen, *Chem. Mater.*, 2007, 20, 110-117.
15. C. Li, J. Yuan, B. Han and W. Shangguan, *Int. J. Hydrogen. Energ.*, 2011, 36, 4271-4279.
16. L. J. Zhang, S. Li, B. K. Liu, D. J. Wang and T. F. Xie, *Acs Catal.*, 2014, 4, 3724-3729.
17. L. Qi, J. Yu and M. Jaroniec, *Phys. Chem. Chem. Phys.*, 2011, 13, 8915-8923.
18. S.-W. Cao, Y.-P. Yuan, J. Fang, M. M. Shahjamali, F. Y. C. Boey, J. Barber, S. C. Joachim Loo and C. Xue, *Int. J. Hydrogen. Energ.*, 2013, 38, 1258-1266.
19. X. Zou, P.-P. Wang, C. Li, J. Zhao, D. Wang, T. Asefa and G.-D. Li, *J. Mater. Chem. A*, 2014, 2, 4682-4689.
20. Y. Peng, Z. Guo, J. Yang, D. Wang and W. Yuan, *J. Mater. Chem. A*, 2014, 2, 6296-6300.
21. L. Ge, F. Zuo, J. Liu, Q. Ma, C. Wang, D. Sun, L. Bartels and P. Feng, *J. Phys. Chem. C*, 2012, 116, 13708-13714.
22. G. Yang, W. Yan, Q. Zhang, S. Shen and S. Ding, *Nanoscale*, 2013, 5, 12432-12439.
23. W.-Y. Cheng, T.-H. Yu, K.-J. Chao and S.-Y. Lu, *Int. J. Hydrogen. Energ.*, 2013, 38, 9665-9672.
24. X. Yao, T. Liu, X. Liu and L. Lu, *Chem. Eng. J.*, 2014, 255, 28-39.
25. W. Zhang, Y. Wang, Z. Wang, Z. Zhong and R. Xu, *Chem. Commun.*, 2010, 46, 7631-7633.
26. Z. Hu and J. C. Yu, *J. Mater. Chem. A*, 2013, 1, 12221-12228.
27. L. J. Zhang, T. F. Xie, D. J. Wang, S. Li, L. L. Wang, L. P. Chen and Y. C. Lu, *Int. J. Hydrogen. Energ.*, 2013, 38, 11811-11817.
28. Q. Li, B. Guo, J. Yu, J. Ran, B. Zhang, H. Yan and J. R. Gong, *J. Am. Chem. Soc.*, 2011, 133, 10878-10884.
29. Z. Yan, H. Wu, A. Han, X. Yu and P. Du, *Int. J. Hydrogen. Energ.*, 2014, 39, 13353-13360.
30. L. J. Zhang, R. Zheng, S. Li, B. K. Liu, D. J. Wang, L. L. Wang and T. F. Xie, *Acs Appl. Mater. Inter.*, 2014, 6, 13406-13412.
31. O. Yehezkeli, D. R. B. de Oliveira and J. N. Cha, *Small*, 2014, DOI: 10.1002/smll.201401490, n/a-n/a.
32. J. Yang, J.-H. Zeng, S.-H. Yu, L. Yang, G.-e. Zhou and Y.-t. Qian, *Chem. Mater.*, 2000, 12, 3259-3263.
33. C. J. Lin, Y. H. Yu and Y. H. Liou, *Appl. Catal. B-Environ.*, 2009, 93, 119-125.
34. J. Jin, J. Yu, G. Liu and P. K. Wong, *J. Mater. Chem. A*, 2013, 1, 10927-10934.
35. J. Yu, J. Jin, B. Cheng and M. Jaroniec, *J. Mater. Chem. A*, 2014, 2, 3407-3416.
36. J. S. Jang, H. G. Kim, U. A. Joshi, J. W. Jang and J. S. Lee, *Int. J. Hydrogen. Energ.*, 2008, 33, 5975-5980.
37. C. Han, L. Ge, C. Chen, Y. Li, X. Xiao, Y. Zhang and L. Guo, *Appl. Catal. B-Environ.*, 2014, 147, 546-553.
38. Q. Xiao, J. Zhang, C. Xiao and X. Tan, *Catal. Commun.*, 2008, 9, 1247-1253.
39. C. Weber, U. Becker, R. Renner and C. Klingshirn, *Z. Physik B*

- *Condensed Matter*, 1988, 72, 379-384.
40. J. Zhang, S. Z. Qiao, L. Qi and J. Yu, *Phys. Chem. Chem. Phys.*, 2013, 15, 12088-12094.
41. J. Tauc, R. Grigorovici and A. Vancu, *physica status solidi (b)*, 1966, 15, 627-637.
42. J. Zhang, Y. Wang, J. Jin, J. Zhang, Z. Lin, F. Huang and J. Yu, *Acs Appl. Mater. Inter.*, 2013, 5, 10317-10324.
43. M. Long, W. Cai, J. Cai, B. Zhou, X. Chai and Y. Wu, *J. Phys. Chem. B*, 2006, 110, 20211-20216.
44. J. S. Zhang, M. Grzelczak, Y. D. Hou, K. Maeda, K. Domen, X. Z. Fu, M. Antonietti and X. C. Wang, *Chem. Sci.*, 2012, 3, 443-446.
45. K. Sing, D. Everett, R. Haul, L. Moscou, R. Pierotti, J. Rouquerol and T. Siemieniewska, *Pure Appl. Chem*, 1985, 57, 603-619.
46. S. Ikeda, T. Takata, T. Kondo, G. Hitoki, M. Hara, J. N. Kondo, K. Domen, H. Hosono, H. Kawazoe and A. Tanaka, *Chem. Commun.*, 1998, DOI: 10.1039/A804549F, 2185-2186.
47. L. Li, P. A. Salvador and G. S. Rohrer, *Nanoscale*, 2014, 6, 24-42.
48. A. Kudo and Y. Miseki, *Chem. Soc. Rev.*, 2009, 38, 253-278.
49. J. Ran, J. Yu and M. Jaroniec, *Green Chem.*, 2011, 13, 2708-2713.
50. X. Chen, W. Chen, H. Gao, Y. Yang and W. Shangguan, *Appl. Catal. B-Environ.*, 2014, 152–153, 68-72.
51. X. Zong, H. Yan, G. Wu, G. Ma, F. Wen, L. Wang and C. Li, *J. Am. Chem. Soc.*, 2008, 130, 7176-7177.
52. K. Chang, Z. Mei, T. Wang, Q. Kang, S. Ouyang and J. Ye, *Acs Nano*, 2014, 8, 7078-7087.
53. H. Yan, J. Yang, G. Ma, G. Wu, X. Zong, Z. Lei, J. Shi and C. Li, *J. Catal.*, 2009, 266, 165-168.
54. X. Zong, J. Han, G. Ma, H. Yan, G. Wu and C. Li, *J. Phys. Chem. C*, 2011, 115, 12202-12208.
55. T. Jia, A. Kolpin, C. Ma, R. C.-T. Chan, W.-M. Kwok and S. C. E. Tsang, *Chem. Commun.*, 2014, 50, 1185-1188.
56. J. S. Jang, D. J. Ham, N. Lakshminarasimhan, W. y. Choi and J. S. Lee, *Appl. Catal. A-Gen.*, 2008, 346, 149-154.
57. R. D. L. Smith, M. S. Prévot, R. D. Fagan, Z. Zhang, P. A. Sedach, M. K. J. Siu, S. Trudel and C. P. Berlinguette, *Science*, 2013, 340, 60-63.
58. S. Cobo, J. Heidkamp, P.-A. Jacques, J. Fize, V. Fourmond, L. Guetaz, B. Jousselme, V. Ivanova, H. Dau, S. Palacin, M. Fontecave and V. Artero, *Nat. Mater.*, 2012, 11, 802-807.
59. M. G. Walter, E. L. Warren, J. R. McKone, S. W. Boettcher, Q. Mi, E. A. Santori and N. S. Lewis, *Chem. Rev.*, 2010, 110, 6446-6473.
60. T. Hisatomi, J. Kubota and K. Domen, *Chem. Soc. Rev.*, 2014, DOI: 10.1039/C3CS60378D.
61. D. Wang, T. Hisatomi, T. Takata, C. Pan, M. Katayama, J. Kubota and K. Domen, *Angew. Chem. Int. Edit.*, 2013, 52, 11252-11256.

Graphical Abstract

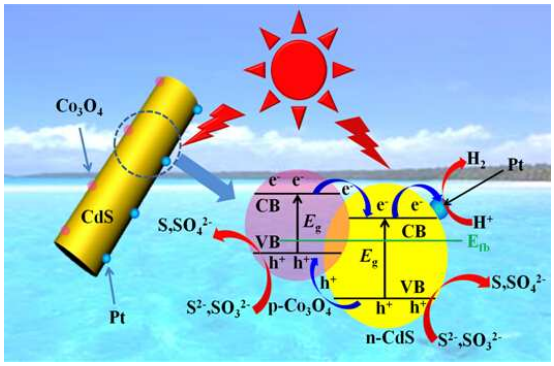


Amorphous $Co_3O_4$ Modified CdS Nanorods exhibit a significantly enhanced photocatalytic activity for $H_2$ Production.